RSC Advances

PAPER

View Article Online
View Journal | View Issue

Cite this: *RSC Adv.*, 2015, **5**, 27313

Electronic pH switching of DNA triplex reactions†

Gabriel Antonio S. Minero,‡ Patrick F. Wagler,‡ Alaa A. Oughli and John S. McCaskill*

Electronic reversible switching of sequence-specific DNA interactions and reactions is an important operation for programming complex molecular and microscopic processes. While both quadruplex and triplex structures are suitable for moderate pH control (pH 5–7), we focus here on the large family of DNA sequences forming pH-sensitive triplex structures. These involve Hoogsteen and Watson–Crick base pairs in pyrimidine–purine–pyrimidine (Y:R:Y) motifs. We demonstrate electronically controlled local pH cycling, integrated into a microfluidic chip, which induces DNA hybridization switching in these triplex complexes. We also show that pH switching can be used to control rapid DNA ligation in double strand templated triplex structures using disulphide linkages. Switching between DNA complexes induced by pH is first characterized using capillary gel electrophoresis before employing local microelectrodes. Robust pH cycling is achieved over a moderate pH range (4–8), by voltage-biased gold microelectrodes immersed in quinhydrone redox systems, both in solution and immobilized on the surface, and is monitored *via* fluorescence ratio imaging with SNARF-4F. The resulting switching of DNA structures (reversible triplex to duplex, triplex-based DNA ligation) based on a hairpin template is spatially monitored by dye–quencher fluorescence. The integration of electronically controlled pH cycling into a microfluidic reactor allows both local patterning of pH and the maintenance of constant ionic strength over many cycles.

Received 10th February 2015
Accepted 9th March 2015

DOI: 10.1039/c5ra02628h

www.rsc.org/advances

Introduction

DNA sequences not only encode biological functions, but also serve as an increasingly versatile platform for sensing, regulating, amplifying, self-assembling and optimizing chemical components and processes. Since N. Seeman's pioneering work, DNA has been recognized as an important agent in nanotechnology,[1,2] its general potential for computation has been widely explored since Adleman's work,[3–5] and it's commercial combinatorial availability has further expanded its role in directing chemical processes.[6] DNA and the oligonucleotide analogues are increasingly being employed as catalysts, encroaching on the classic functional domain of proteins as in the RNA world.[7] While enzyme-free replication of DNA has proved remarkably difficult to extend to longer sequences[8,9] as a constructive (bond forming) process, autonomous DNA amplification processes involving strand displacement and conformational transitions[10] or the formation of DNAzymes[11,12] are now known. In this work, we address the problem of gaining electronic control of such complex processes in spatially resolved systems. The ultimate goal of this work is to provide an enabling technology for building electronic chemical cells,[13] linking electronic information processing with self-organizing chemical systems, but in this paper we focus on gaining full electronic control under mild conditions of low ionic strength for two of the basic DNA processes underlying the above developments: DNA hybridization and ligation. To this end, we make use of known pH dependent triplex conformations of DNA.

Triplex DNA is known for switching certain genes on and off in living organisms by influencing the binding of DNA polymerase with its promoter.[14–16] Stressed double stranded DNA can undergo regroup into triple stranded form called H-DNA,[17] widely found in the screening of mammalian genes. It was shown[18] that supercoiled plasmid DNA undergoes such changes of DNA conformation forming purine (R:R:Y) and pyrimidine (Y:R:Y) triplex motifs in the presence of Zn^{2+} and H^{+} ions respectively. Since the pK_a of the imino group of cytosine bases is between 5 and 6, the charge of these residues, and hence the potential for Y:R:Y triplex interactions, is strongly pH-dependent.[19] Stability of the Y:R:Y triplex DNA motif relies on the TAT and CGC^{+} Hoogsteen triplets, and, therefore, pH affects the potential for the Y:R:Y sort triplex interactions. Although the positive charge of cytosine bases decreases the repulsion of strands upon Hoogsteen binding, it has been shown that triplex formation also requires a significant counter ion (Na^{+}, Mg^{2+}) concentration[19–22] or polyamines.[23,24] A reversible switching

Faculty of Chemistry and Biochemistry, Microsystems Chemistry and BioIT (BioMIP), Ruhr-University Bochum, 44780 Bochum, Germany. E-mail: john.mccaskill@rub.de

† Electronic supplementary information (ESI) available: This includes structural information, spectroscopic observations of triplex DNA as well as its conformational transitions, CGE conformational analysis, preparation methods of pMBQ modified surfaces, electrochemical pH cycles on a chip, and supplementary figures. See DOI: 10.1039/c5ra02628h

‡ Equally contributing authors: Gabriel Antonio S. Minero and Patrick F. Wagler.

between triplex and duplex structures has been observed on varying pH between 5.0 and 8.0.[25–27]

DNA triplex recognition has been employed to regulate various functions of biosystems, as it does not require the melting of existing double stranded DNA for sequence recognition.[28] Switchable DNA nanostructures[29] show the potential to be exploited in *in vitro* engineered systems, for example as information storage devices or nanoscale circuits.[30] Acid-driven assembly of the triplex-gold nanoparticle conjugates[31] could be arranged into a delivery system for small molecules, that is switchable by the pH-dependent structural change of triplexes. A triplex DNA nanomachine[25] which consumes small ions, H^+ and OH^-, would be compatible with protein ion channels, that control pH by switching between closed and opened states. Several systems involving triplex formation show robust repeatable cycling of pH switching, as confirmed by the FRET studies[25,27,29] and photocurrent studies.[30] Y:R:Y triplex DNA has the great advantage that only small changes in pH are sufficient to reverse the stability of hybridization, without risk of destructive depurination of DNA (<pH 4) or cleavage, as compared with the mM concentrations required for ds DNA (*e.g.* pH 12). Similarly sensitive switching is also observed for DNA quadruplexes.[32–34] On the other hand, a gradual increase in the ionic strength, *e.g.* as a result of the accumulated NaCl in acid–base titration with NaOH and HCl, changes the performance of a triplex switch as evidenced by the formation of irreversible aggregates.[31] Natural autonomous purely chemical pH oscillators are appealing[35–38] but do not themselves enable external switching or control of DNA processes, which is the main motivation here. They also suffer from compatibility and stability issues when combined with other chemical processes, and they cannot easily be modulated in period or amplitude in real time.

Many functional roles of triplex DNA, such as in the assembly of nanostructures[25,29,39] and in the construction of nanomachines[25] and networks[31] have been shown. We are exploring its further use in connection with a self-replicating DNA system, using palindromic homopurine (R) and homopyrimidine (Y) DNA to provide triplex and duplex DNA ligation series upon pH switching.[40] Since Nicolaou's paper in 1994, a considerable effort has been devoted to the development of more rapid ligation chemistry involving end-selenated[41] as well as end-thiolated[42] DNA oligonucleotides. Recently a novel fast ligation chemistry involving templated disulphide bond formation was presented.[43] In that work, to follow triplex DNA ligation, a dye–quencher pair on the same DNA strand was employed, with the quencher being released as a leaving group by the ligation reaction. This labeling scheme is also employed for the triplex templated ligation reaction reported here as an electronically switchable complex. Ultimately, such pH controlled complexes may be useful in controlling product inhibition and establishing a triplex based self-replication scheme which makes use of pH cycling without titration, but this is beyond the scope of the current contribution.

The quinhydrone redox system has been established as a robust method to induce pH changes in a controlled manner in pH sensor and related devices[44] as well as in microfluidic systems[45] at potentials significantly lower than those involving water electrolysis (*e.g.* 1.23 V *vs.* SHE). Even at moderate potentials, above this threshold, such a system allows most of the current required to maintain electrophoresis to flow without electrolysis and associated gas formation. Voltage biased microelectrodes have been shown to cause pH changes in their surroundings in such a redox mixture. This system has the advantage that multiple pH cycles on a chip did not require refilling of the microchannel with fresh redox mixture and were performed in sequence, which is important for practical applications to DNA processing in microfluidic systems. The characterization of spatial and temporal changes in pH gradients in microfluidic systems has also been performed using a bead-immobilized pH-sensitive fluorescent dye[46] or polymer microcapsules loaded with a pH-sensitive fluorophore,[47] which act as mobile sensors within the microchannels. In this work, we compare the performance of immobilized and in solution quinhydrone redox couple, and monitor pH using ratio imaging of the dye SNARF-4F (see also Materials and methods section). We employ both same channel and remote channel pH switching, and use the latter to control the triplex-based ligation of DNA. The amount of the product ligated in the vicinity of the microelectrodes orchestrating pH changes was sufficient to be detected by fluorescence changes. Proximal as well as remote DNA ligation was triggered electronically in a microchannel.

Local electrodes not only can initiate redox chemical reactions but also can contribute to directed electrokinetic transport of DNA and other charged molecules *via* electrophoresis and electroosmosis. Such transport processes can also play an important role in processing DNA in microfluidic structures, so in order to first separate them from the effects of Faradaic reactions (such as modulated pH) we also established a multi-segment capillary gel electrophoresis (CGE) technique with multicolour laser induced fluorescence detection but without local electrodes. This enabled the kinetics of triplex formation during transport to be separately determined and facilitated the analysis of complex DNA equilibria, such as those arising during triplex-based DNA ligation. Fast separation as well as online monitoring of DNA was achieved in Pluronic® thermoresponsive gel matrix,[48] which as a reversible gel also allows further integration of this fractional analysis of DNA complexes with microfluidic channels.[49]

Following the Materials and methods section, the main results of the paper are presented, relegating supporting and background experimental data to the ESI.† Firstly, a spectroscopic analysis and comparison of the intermolecular Y:R:Y with the hairpin/single stranded H:Y triplex complexes are presented. In particular, the pH dependence of the triplex and duplex systems for these two cases is analysed. We then characterize the local electronic cycling of pH using microelectrodes in microfluidic channels, comparing both the surface bound and free hydrobenzoquinone systems, and demonstrating effective pH switching both in channel and in a remote passive channel. Thirdly, we present our main results on the local electronic cycling of triplex binding *via* pH. The final results section shows how remote pH switching can be used to switch fast triplex-templated ligation *via* electronic control. Further

results and background information can be found in the ESI.† The paper finishes with a discussion of these results and with the conclusions that can be drawn from this work.

Materials and methods

DNA sequence design

The sequences employed are listed in the Table 1. The structures of complexes and their roles are shown in ESI, Fig. S1.†

DNA sample preparation

The DNA triplexes Y:R:Y, H:Y and H:Q were formed by mixing corresponding strands in the ratios 2 : 1 (ss **Y24** : ss **R24**) and 1 : 1 (ss **Y24** : ds **H24**), respectively, in the standard hybridization buffer (10 mM phosphate buffer, 50 mM NaCl) at various pH values. The systems were annealed at 90 °C and properly hybridized while cooling to 25 °C over 90 min (thermomixer Eppendorf). Alternatively, mixtures were kept at room temperature for 1–24 hours. We investigated the pH-dependence of triplex formation within the pH range 5.0 to 7.5. In order to avoid chloride ions, due to the possible etching of gold microelectrodes, we used 1–100 mM sodium phosphate (KMF) in experiments on the microfluidic chip. To monitor the pH-driven DNA triplex switch we used Alexa488, Alexa647 as well as BHQ-3 end-labelled DNA (Table 1). DNA oligonucleotides **Y24**, **R24**, **H53**, **F12** and **Q24** were ordered at IBA (Germany) with double HPLC purification grade and the stock concentration of 100 μM. Concentrations of oligonucleotides were double-checked using a Nanomag absorption spectrometer (IMPLEN). S-modified DNA oligonucleotides **P12** and **S12** were synthesized by V. Patzke (Ruhr-University Bochum, Germany).[43]

UV-melting analysis

Spectrophotometric melting curves were measured at pH 7.5, 6.0 and 5.0 in order to verify suitable temperature range for pH-driven switch of DNA conformation. Prepared samples of 1 μM concentration were placed into Varian Cary UV-visible spectrophotometer, in a quartz cuvette with 10.0 mm optical path length (Hellma, Germany). Thermal denaturation and renaturation profiles were obtained upon cycling temperature between 15 °C and 90 °C. Thermal equilibration of complexes was achieved by annealing at a constant rate 0.5 °C min^{-1} after holding samples at 90 °C for 3 min. UV absorbance measurements were performed at 260 nm. Integral melting curves were smoothed with moving average (5 points).

Table 1 List of DNA oligonucleotides employed

DNA code	Complexes / role	DNA sequence 5′ to 3′	Modification (M_w in g/mol)
Y24	ss, ds, ts	CCC TTC CTC TTT TTT CTC CTT CCC	5′-Alexa647/488
R24	ss, ds, ts	GGG AAG GAG AAA AAA GAG GAA GGG	5′-Alexa488
H53	DNA hairpin, ts	CCC TTC CTC TTT TTT CTC CTT CCC TTTTT → GGG AAG GAG AAA AAA GAG GAA GGG ←	5′-Alexa647
F12	ss, ts	CCC TTC CTC TTT	5′-Alexa488
Q24	ss, ts	CCC TTC CTC TTT TTT CTC CTT CCC	3′-BHQ3
P12	ss, ts	CCC TTC CTC TTT	5′-Alexa488, 3′-S-Dabcyl
S12	ss, ts	TTT CTC CTT CCC	5′-SH

CD conformation analysis

CD spectra were recorded at pH 7.5, 6.0 and 5.0 in order to verify DNA structures formed in the annealed as well as isothermally prepared systems. Samples of 5 μM and 1 μM concentration were placed into a spectropolarimeter (JASCO J-715; Japan with a xenon lamp) in quartz cuvettes with 0.5 mm and 10.0 mm optical path length (Hellma, Germany), respectively. In order to prevent attack from oxygen radicals under UV irradiation, constant nitrogen flow was arranged using a water bath (Haake Co., Germany) at 20 °C. The temperature of the cuvette location was adjusted to 20, 30, 40, 50, 60, 70 and 90 °C using a JASCO PTC-4235 temperature controller. CD spectra were recorded in the wavelength range 200–350 nm with 1 nm data pitch, 10 nm min^{-1} scan rate and 1 s response time. The measurements were accumulated 5 times and smoothed after background subtraction using a 9-point Savitzky–Golay model.

Capillary gel electrophoresis

Fast DNA separation was performed in a capillary filled with 25% Pluronic F127 gel in 50 mM Tris–acetate buffer at 25 °C. A capillary (ID 75 μM, OD 360 μM) was placed under a fluorescence microscope (see below) between two reservoirs buffer solutions, with a detection window exposed to the objective as well as laser illumination (488 and 640 nm, see below). Two platinum wires were introduced into the buffer solutions, supplying the system with current. For injection of DNA we replaced buffer by sample solutions, and applied 600 V potential (Invitrogen power supply) for 5 s (measured current 40–60 μA). For DNA separation, we substituted sample solution after the injection with pure buffer and applied constant 600 V potential. DNA migrated in the separation media from cathode to anode and different DNA complexes (ss, ds or ts DNA) were detected in the detection window using several regions of interest (ROIs) with laser-induced fluorescence of Alexa488 and Alexa647. Both dyes gave stable fluorescent signals over time, which were pH independent over a wide range (4–10). Two lasers were switched automatically (using an AOTF) and the images were sorted during the acquisition process. The fluorescence intensities were taken with an EMCCD-camera (iXon, Andor Technologies) and normalized. The exposure time was 1–2 s.

Fluorescence spectroscopy analysis

Fluorescence spectra in the range 620–800 nm were obtained with monochromatic light excitation at 600 nm (Xe lamp) with a scan rate of 100 nm min^{-1}. Samples containing 0.5–1.0 μM Alexa647-labeled hairpin DNA ds **H24** as well as BHQ-3 labelled

ss **Q24** were used for online monitoring of pH cycles involving ts **HQ** formation and its dissociation *via* pH change. Aliquots of 2 M HCl and 1 M NaOH were added to 500 μl of a sample sequentially in order to obtain square-wave fluorescence changes for the pH-titrated triplex switch. Samples containing 0.5 μM, 1.0 μM and 2.0 μM of ds **H24** in the hybridization buffer were mixed with aliquots of ss **Q24** up to its final concentration of 0.5 μM, 1.0 μM and 2.0 μM, respectively, for investigation of triplex kinetics. Prepared samples were introduced into a luminescence spectrometer (Aminco Bowman Series 2, USA) in a cuvette with 10.0 mm optical length path. Fluorescence values at 668 nm were recorded online over time with a 30 s sampling interval. The time gap between final mixture preparation in a cuvette (change of pH or addition of third strand) and measurement was 5–10 s.

Microfluidic fabrication and custom microelectrode array chips

The microfluidic chip used for our investigation contained a silicon substrate with integrated gold electrodes and a micro-moulded fluidic layer, which consists of a network of channels and microreactor compartments. For fabrication and various designs of these microfluidic systems as well as proof-of-principle experiments for laser-driven fluorescence detection of biomolecule processing see.[13,50–52] Multilevel microfluidic channels and compartments were micro-moulded in PDMS (polydimethylsiloxane, Sylgard 184) after the prefabrication of an SU-8 master using standard soft-lithography methods. PDMS has excellent optical properties for a fluorescence-based detection, due to the fact that it has almost no absorbance and minimal auto-fluorescence in the range of visible wavelengths.[53] PDMS enjoys wide usage in the field of biochemistry and fabrication for biological studies.[54,55]

Microfluidic methods

The microreactor (Fig. 1) was connected to FEP capillary tubes (Fluorinated Ethylene Polymer, ID/OD: 200/800 μm ScanTube GmbH, Germany) *via* a custom PDMS multiport connector.[56] Prior to use, the microchannels were checked for blockages and leaks by pumping water using 1 ml syringes (Henke Sass Wolf) and needles (B. Braun) connected to the inlets *via* a *ca.* 1 cm silicon adapter (Carl Roth GmbH, ID 0.5 mm, OD 2.5 mm). For precise flow control, 50 μl Hamilton syringes were connected to pulse-free syringe pumps (MMT Micromechatronic Technologies GmbH Siegen). The redox mixture containing labelled DNA strands **H24** and **Q24** (1 μM) was pumped at a flow rate of 100 μl h^{-1} until the fluid-switch air bubble appeared, then the flow was reduced to 10 μl h^{-1} until the whole channel was filled with fluorescent DNA. Finally, the flow was either stopped or reduced significantly (min. 0.3 μl h^{-1}), depending on the experiment. The microchannels were cleaned with water (30 min, 100 μl h^{-1}) using a syringe pump (TSE Systems Gmbh). In case of contamination of the PDMS surface by organics, it was reactivated using an $HCl/H_2O_2/H_2O$ mixture (5 min) followed by a 30 min aqueous washing step.

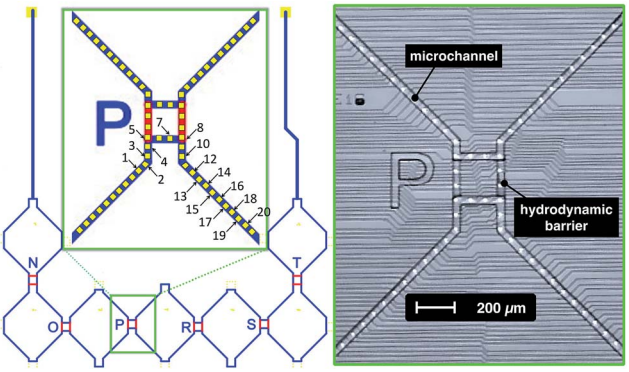

Fig. 1 Microfluidic design of the electronic pH switch for triplex DNA. Left: overall microfluidic layout schematic and blow-up showing microelectrodes. Substructures N–T had a similar microelectrode pattern as well as microfluidic map, structure P is blown up as an example of one of the used substructures. Right: detailed image of microreactor. Top and bottom microchannels (35 μm) were connected *via* 1 μm deep hydrodynamic barriers. Microelectrodes are numbered as 1 to 20. In the experiments related to the H-structure, the electrodes 1–12 were used. For cycling of voltage, the electrodes 12–20 were employed. The regions of the side channel monitored in the 10× microscope objective were located upstream, downstream as well as in between the active microelectrodes.

We refer to the core microfluidic substructure (see blow-up in Fig. 1) as a (double) H-structure. The two hydrodynamic barriers served to prevent mixing of solution contents between the two parts under limited pressure differences. The double H-structure was monitored using 10× and 20× objectives (see below). The pH and triplex cycles were monitored in the side channel of the H-structure (Fig. 1) in an area containing nine 20 × 20 μm microelectrodes. We used the same sub-structure in the same microchannel as much as possible in order to minimize errors. Analysis was done on the image and time course data obtained with custom acquisition and control software (*ng_biopro* see below).[57]

Redox reactions causing pH changes and further downstream reactions were executed on the chip after the flow was stopped. Patterns of pH in microfluidic chip array were produced electronically using the quinhydrone (QH_2) to benzoquinone (Q) redox system.[58]

$$QH_2 + 2OH^- \leftrightarrow Q + 2H_2O + 2e^-$$

The microfluidic channel map as well as the map of microelectrode locations were loaded in the *ng_biopro* software to allow specific microelectrodes to be biased *via* interactive graphical selection, as illustrated in the Fig. 4–6, and 8. Uncontrolled changes of pH towards values more than 9.0 were avoided because of possible silicon dioxide damage.

Electrode and imaging control system

Custom software[57] was used to control electrodes and pumps, take images from a high resolution EMCCD-camera (iXon DV885, Andor), and record averaged intensities at certain regions of interest (ROI). Electrodes were driven directly by

FPGA output drivers with voltages ranging from 1.2 V up to 3.3 V in discrete steps.[52] The pulse-frequency of the electrodes range from DC up to a few MHz. Three electrode states were employed: GND (0 V), tristate (high impedance) and VDD (fixed discrete values chosen from 1.2 to 3.3 V). To reduce the average rate of electrolytic gas formation, a pulse-code-modulation was applied with an active-duty-cycle from 0% to 100%, specifying the relative width of the active pulse in each cycle. In the non-active part of the duty-cycle the electrodes were set to tristate.

The performance of the electrodes was tested periodically using an electrochemiluminescence (ECL)[59–61] solution, based on a buffered electrolyte solution (0.1 M phosphate buffer, pH 6.9) containing 5 mM $Ru(bpy)_3^{2+}$ and 25 mM tripropylamine (TPA) and 100 μM benzyl viologen. The TPA radical serves as a reductant, facilitating the $Ru(bpy)_3^{2+}$ catalyst return to its base state following light emission. The emitted ECL signal around 610 nm can be easily detected using a digital camera. This method allowed a direct optical control of microelectrodes with a fast response time, which is useful for performing quality control, and helpful *e.g.* in finding electrical conduction defects.

Fluorescence images of the labelled DNA fractions as well as SNARF-4F pH-indicator were recorded *via* the EMCCD camera (see above), producing low-noise video rate images (1002 × 1004 pixels) that are readout and processed with *ng_biopro* software. The laser-induced fluorescence imaging was performed with an inverse microscope (Olympus IX81, objectives: 4×, 10×, 20×, 63×) and a custom confocal line-scan illumination option using cylindrical optics, a galvoscanner (*X*-axis of Thorlabs GVS002 XY scanner with >5 mm aperture, Becker and Hickel GD120 scanning controller) and two lasers at 488 nm (100 mW cw, coherent sapphire 488–100 CDRH) and 640 nm (100 mW cw, coherent cube). A single quad-line (Semrock CSUX 405/488/561/640 nm) laser-line blocking emission filter was used in all experiments. In addition, specific emission filters with carboxy SNARF-4F (see below) for pH. The location of the regions of interest were adjusted using an *XY* stage (H117N2IX Proscan, Prior Scientific Instruments GmbH).

Ratio imaging of SNARF-4F as pH indicator

In order to monitor pH changes we used carboxy SNARF-4F (Molecular Probes), a dual emission fluorescent dye, at two emission wavelengths, λ_{em}, 580 and 640 nm. SNARF-4F, 232 μM, was diluted to the final concentration 10, and 50 μM. A series of SNARF-4F samples in the phosphate buffer at different pH (5–9) were produced on a microtiter plate (Corning) and exposed to 488 nm laser light, *ca.* 3 mW for 0.5 s, while emission filters were switched between 565–605 nm (585/29 nm BrightLine® single-band bandpass filter FF01-585/29-25) and 660–740 nm (700/75 nm ET Bandpass) with a frequency 0.25 Hz (fluorescence monitoring time frame 4 s per filter).

Ratio-images of SNARF-4F fluorescence recorded at two different wavelengths, were calibrated against pH by plotting the ratios I_{700}/I_{585} *vs.* pH (Fig. 2) using the following equation (Molecular Probes Product Information):

$$\mathrm{pH} = \mathrm{p}K_a - \log\left[\frac{R_B - R}{R - R_A}\right] - \log\left[\frac{F_{B(\lambda 1)}}{F_{A(\lambda 1)}}\right] \quad (1)$$

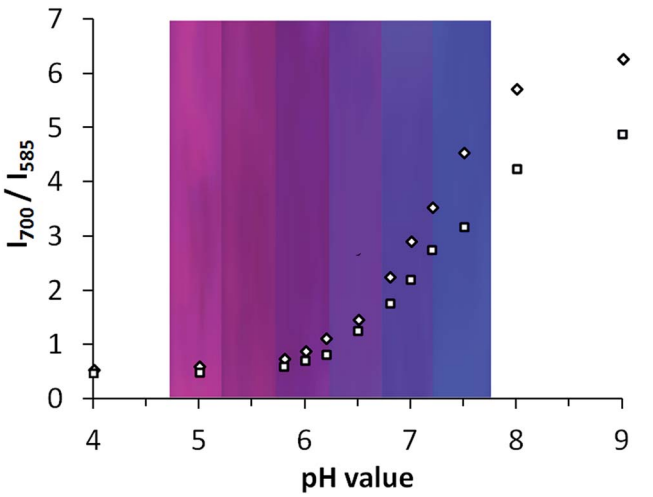

Fig. 2 Titration of SNARF-4F fluorescence ratios against pH in bulk solution (eqn (1)) for 10 μM (rhomboids) as well as 50 μM (squares) dye concentrations. The colour bar represents output of the fluorescence ratio images in the working pH range 5–7.5 (blue colour – 660–740 nm, pink colour – 565–605 nm), acquired in the microchannel and processed *via* Fiji.

with the pK_a value of 6.4, while R_A and R_B were taken from Fig. 2 for 10 μM SNARF as 0.5 and 5.0, the ratios I_{700}/I_{585} at the threshold acidic and basic pH, and $F_{B(\lambda 1)}$ as well as $F_{A(\lambda 1)}$ were taken from the titration plot at 585 nm. A red shift of the dye emission occurred for increasing pH. The pH values were set and maintained in a 50 mM phosphate buffer.

Electrode modification by pMBQ in the microreactor

A gold disk electrode (3 mm diameter) was used as a reference substrate for immobilization of *para*-mercaptobenzoquinone (pMBQ). The modification steps as well as electrochemical characterization of the gold surfaces (disk electrode as well as microelectrodes on a chip) are shown in the Fig. S5.† Before any modification, the substrate was grinded and polished (with 1 μm, 0.3 μm and 0.05 μm alumina slurry). The disk electrode was coated with pMBQ by dipping it in an aqueous solution of pMBQ (10 mM) over night (argon treated to remove dissolved oxygen prior to adding pMBQ). Electropolymerization of pMBQ using 0.2 mg ml^{-1} of pMBQ dissolved in phosphate buffer (0.1 M, pH = 7.2) was carried out on the pMBQ-functionalized disk electrode by the application for 50 min of a constant potential (*E* 0.6 V *vs.* Ag/AgCl (3 M KCl) with Pt wire as counter electrode). Afterwards the electrode was washed with phosphate buffer. The newly modified electrode covered with a layer of the pMBQ was tested with cyclic voltammetry at scan rates of 25, 50, 100, 200, and 300 mV s^{-1} in phosphate buffer (0.1 M, pH 7.2) *versus* Ag/AgCl reference. All electrochemical measurements on the disk electrode were accomplished using a *Gamry Reference 600* potentiostat.

The microchip with its gold microelectrode array was then modified with pMBQ by coating its surface with aqueous solution of MBQ (10 mM) over night. For the electropolymerization of pMBQ on the surface of gold microelectrodes pre-coated with

pMBQ we connected the microreactor to potentiostat (μ-Autolab III FRA, Deutsche Metrohm GmbH & Co. KG). For this purpose we split the overall number of microelectrodes into groups of working, counter and pseudo-reference electrodes. Then the electropolymerization was performed on the chip by applying a potential of 0.6 V over 50 minutes where 600 microelectrodes were used as working, 600 as reference and 1800 as counter electrodes. Subsequently, the surface of the chip was gently washed with phosphate buffer and the newly modified microelectrodes were tested using cyclic voltammetry at scan rates 50 and 100 mV s^{-1}. The same electrode distribution as above was used and the measurements were done in phosphate buffer solution (0.1 M, pH 7.2).

Bulk pH changes

A stock solution of 0.6 M hydroquinone/0.6 M benzoquinone redox system was prepared in a 30% methanol–water mixture. This redox mixture was diluted to 30 mM working concentration in 1–100 mM phosphate buffer. Subsequently, electronically biased pH values were assigned using SNARF-4F in selected areas of the microfluidic channel (Fig. 1): upstream of the microelectrode 12, between 13 and 14 as well as between 18 and 19, and downstream of 20. The electrodes 12–14 were at the same polarity (positive) while the electrodes 18–20 were at the opposite polarity. The polarity of the microelectrodes, 12–14 *vs.* 18–20, was cycled between positive and negative. Two areas containing six active (1.8 and 2.5 V) microelectrodes were separated by three tristate microelectrodes. For remote pH-changes two ROIs were monitored, between electrodes 6 and 7 in the bottom channel as well as in the top channel.

The extent of pH changes was assigned *via* SNARF-4F fluorescence analysis using ratio imaging (see above). Fluorescence was integrated over two different ROIs located near the −ve and +ve active microelectrodes. To maintain pH oscillations within the 5 to 7 range we used a 50 mM phosphate buffer. At this ionic strength, in a system without flow, pH values could be driven periodically on the time scale of minutes under the control of external potential. A large amplitude pH oscillation was found at 1.8 V, and this value was used in subsequent experiments. At 2.5 V (data not shown), the oscillations of pH gradually shifted towards lower values, most likely through irreversible processes, for example, associated with loss of the benzoquinone component in PDMS due to its hydrophobic nature. In fact, post reactivation of PDMS reproducibly revealed displacement of benzoquinone from the channel.

The same electrode configuration and microfluidic channel (Fig. 1) was then chosen for monitoring triplex cycles. Under optimal pH control (stopped flow, 30 mM quinhydrone system, 50 mM phosphate buffer) strands ds **H24** and ss **Q24** were switched between duplex and triplex, and pH cycles were monitored as oscillations of fluorescence of Alexa647. Both molecular DNA components, ds **H24** and ss **Q24**, were mixed in the phosphate buffer (DNA final concentration 1 μM) containing quinhydrone redox mixture and subsequently pumped into microfluidic channel at a flow rate of 50–100 μl h^{-1}. When fluorescence appeared in the microchannel the pumps were switched off and the experiments performed after 30 min relaxation time as described above, following fluorescence at 647 nm excitation.

Electronic disulphide based DNA ligation

DNA ligation was performed according to a recent publication[43] but using triplex complexes rather than double stranded complexes for templating. DNA hairpin ds **H24** served as the template for the disulphide ligation of DNA ss **P12** and ss **S12** within triplex DNA (see Table 1). Concentrations of the strands were 1.0 μM, 0.5 μM and 2.0 μM, respectively. DNA ligation was checked separately in the bulk and the band of 24-mer ligated product was monitored in 12.5% PAAG (50 mM TA buffer, 220 V).

The double H-structure (Fig. 1) was subsequently used for electronically controlled DNA ligation in the microchannel. Ligation relied on the electronically biased pH changes monitored in the 30 mM quinhydrone redox mixture/50 mM phosphate buffer. Microelectrodes were biased at 1.8 V: electrodes 1–4 and 9–12 negative, 5–8 positive. The SNARF-4F fluorescence reflecting changes in pH, was monitored in the H-structure over 1 h with constant potential in the bottom channel. Afterwards, pH relaxation was monitored over 1 h, when the electrodes were turned off. The strands ds **H24**, ss **P12** and ss **S12** in the redox mixture/phosphate buffer were subsequently transferred to the microchannel and the ligation of strands ss **P12** and ss **S12** was monitored in the stationary microfluidic system *via* fluorescence under the same 12 electrode pattern. Up to 70% of active duty of 10 s voltage cycle was applied. DNA ligation was also monitored under flow conditions (0.3 μl h^{-1}) arranged so that the top part of the microchannel was not accessible to the flow, and the flow in the bottom part was about 0.6 μl h^{-1}. Two ROIs were monitored: between electrodes 6 and 7 in the bottom channel and in the top channel of the H-structure (Fig. 1). Fluorescence intensities from the Alexa488 label were recorded over time and the fluorescence enhancement over 1 h was calculated. The efficiency of ligation was estimated by fluorescence changes in the presence of the template in contrast to the non-templated fluorescence changes.

Results

Triplex–duplex equilibria, mobilities and dissociation during transport

In this section we compare the binding equilibria and non-equilibrium fractionation of complexes during transport for both the full trimolecular triplex system (Y:R:Y) and the bimolecular model system (H:Y) involving the RY hairpin (H). It is well known, that the thermodynamic stability of triplex DNA interactions is strongly dependent on the buffer content, such as salt concentration, additives and pH.[20] Moreover, DNA modifications such as dye labels can also change affinity between strands.[22,62] Whereas UV and CD spectroscopic methods allowed us to study equilibria between DNA strands, we also investigated the disproportionation of molecular complexes during strand separation, since reveals kinetic

information, because transport of DNA can be used as an essential component of triplex based DNA replication schemes.[49] We intentionally designed our triplex oligonucleotides ss **Y24** as well as ss **R24** with an overall structure similar to the previously reported one used to investigate triplex-based DNA replication.[40] The hairpin DNA template ds **H24** enables simpler (bimolecular) binding equilibria, clearer control of triplex labelling as well as better thermal stability of the ds template[63] (see also ESI Fig. S1–S4†).

In the initial experiments (see ESI†), we compared two methods of formation of the triplexes, *via* annealing and isothermally in 10 mM phosphate buffer and 50 mM NaCl (see Materials and methods section). The lower salt conditions (*cf.* 1 M NaCl for standard thermodynamic studies) were used for compatibility with enzymatic ligation. The results obtained from spectroscopic measurements indicated the formation of stable triplex DNA in both systems at pH 5–6 within the working temperature range of 25–30 °C (Fig. S2†). Labelling of the strands revealed destabilization of ts Y:R:Y and an isothermal triplex–duplex transition near pH 6 (shown by CD, Fig. S3†). The hairpin system H:Y, labelled on the both strands, underwent an isothermal triplex–duplex transition shifted to higher pH value (*ca.* 7). The stabilities of triplexes Y:R:Y and H:Y were different as trimolecular *vs.* bimolecular complexes.

Complex binding during transport was then studied in the CGE setup, DNA triplexes were separated from hairpin-duplexes and single strands as monitored by laser induced fluorescence of two dyes Alexa488 and Alexa647 (ref. 64) on the separate species. CGE was employed for complexes formed by annealing as well as for isothermally mixed DNA strands. While both preparations of H:Y demonstrated the presence of a peak attributed to the triplex by two-colour detection (Fig. 3 and S4†), complete binding was only achieved upon annealing of the whole DNA constructs. There was only one peak (t = 480 s) identified on CGE plots by fluorescence signals from both DNA bound fluorophores, Alexa647 as well as Alexa488. The peak can be assigned to ts HY as it is identified by two colours in the right ratio and also because it occurred only at pH ≤ 6.0 (Fig. S1A†).

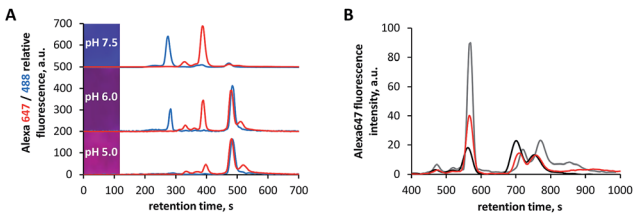

Fig. 3 DNA complex CGE with 2-color laser-induced fluorescence detection. CGE uses Pluronic block-copolymer matrix (see Materials and methods). (A) CGE analysis of temperature annealed samples at different pH with overall separation time less than 10 min at different pH. DNA complexes were identified accordingly to the fluorescence outputs as ss **Y24**, ds **H24** and ts H:Y. Driving current 65–67 μA, the colour scheme for pH is taken from Fig. 2. (B) CGE analysis of non-annealed systems H:Y containing different equivalents of template hairpin **H24** and ss **Y24** at pH 5.0: 1 : 1 (red), 1 : 2 (black), and 2 : 1 (grey), respectively. Driving current 41–42 μA. DNA complexes were identified according to the fluorescence outputs as ss **Y24**, ds **H24** and ts H:Y.

There was no peak broadening observed during separation (triplex retention times 450–720 s). For H:Y, fully annealed at pH 5.0, we did not detect free **Y24**. A low amount of free **Y24** was observed at pH 6.0 and the full amount of excess unbound ss **Y24** was detected at pH 7.5 (Fig. 3A). Since unbound **Y24** was observed even when present in double excess at pH 7.5, the triplex DNA structure, identified in CGE as the slowest electrophoretic mobility peak, was indeed pH switchable to the duplex and single strand form.

The results confirm the reversible formation of triplex DNA and the stable migration of triplex complexes under weakly acidic conditions. A shoulder near the triplex peak was detected only in red fluorescence, *i.e.* not involving **Y24**. It must be related to another complex involving only **H24**. While a two-fold excess of the third strand **Y24** improved the triplex yield (Fig. 3B, measured using areas under the peaks), a two-fold excess of template did not (65% and 45%, respectively, compared with 50% under isothermal conditions). Apparently (see Fig. 3B), the excess of ds **H24** contributes to alternative complexes/conformations at high concentrations.

Immobilized and free redox systems for the remote electronic control of pH changes on a microfluidic chip

While the quinhydrone redox couple is well established for inducing controlled pH changes in microfluidic chips,[45] the charged species involved can be transported and concentrated inhomogeneously under the electric fields employed for electrophoresis. To better distinguish such potential effects, we first investigated an immobilized version of this system as a control (for the synthesis and characterisation see Fig. S5†). In the immobilized sulphur-substituted hydrobenzoquinone system, the process of generating/consuming protons by redox reactions was localized in the vicinity of self-assembled monolayers of pMBQ on the gold microelectrodes.

The initial tests of pMBQ system immobilized to the microelectrodes on a chip were performed in a sealed pure aqueous film (depth 0.5 mm, Fig. 4A). The system had very fast response; the driven switch of pH was reproducible between 5.7 and 6.3 as observed for 9 cycles, with a slight calibration drift of 0.1 pH units (Fig. 4B).

Subsequently, the thickness of the SNARF-4F dye film over the microchip was decreased to *ca.* 30 μm using microbeads (d = 30 μm) as spacers (Fig. 4C). This corresponds to typical film thicknesses in microfluidic systems. In the thin-film system we observed significantly larger pH changes, as expected for higher surface/volume ratios. The pK_a value of SNARF-4F dye is around 6.4; therefore, strong pH changes can also affect its net charge. As expected from the carboxyl group, it was repelled from the cathodes and attracted to the anodes. At very low pH, fluorescence becomes very weak explaining the dark circles appearing reproducibly in the vicinity of anodes (Fig. 4C). The plot (Fig. 4D) shows strong pH changes (*via* calibration curves, see Materials and methods for details) when reversing the electrode potential. Oscillations in pH from 7.4 down to 5.8 or even 5.4 were observed near the switching microelectrodes. In summary, a change in pH of 1.5–2.0 units was electrically induced in this

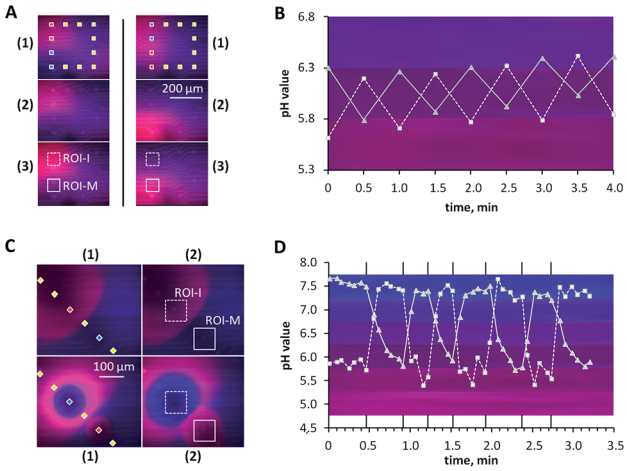

Fig. 4 Reversible pH switches near microelectrodes in the microreactor containing immobilized pMBQ. (A and C) Show ratiometric fluorescence images of SNARF-4F pH indicator over the microelectrode arrays. Image frames (1–3) were acquired with 10 s data pitch (before and after inverting potential of the biased microelectrodes). Two ROIs were monitored over multiple potential switches at 1.8 V. (B and D) Illustrate values of pH assigned at two ROIs *via* SNARF-4F (see Materials and methods). The microreactor thickness was varied between *ca.* 500 μm (A and B) and 30 μm (C and D). The colour scheme used to report pH is calibrated as shown in Fig. 2 and used throughout this paper. The oscillated values of pH are resolved into two coloured areas corresponded to the switched electrode polarity.

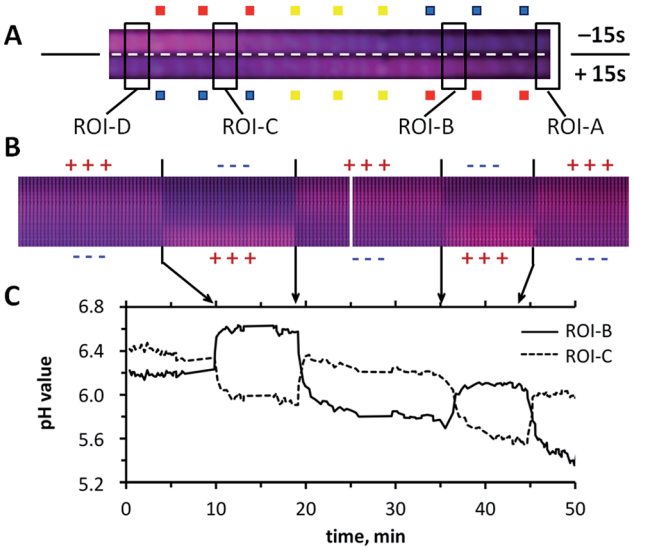

Fig. 5 Fluorescent pH indicator implemented to the custom microfluidic pH oscillator. Changes of pH induced by the redox reaction of benzoquinone/hydroquinone were monitored with SNARF-4F fluorescence *via* dual emission analysis at 700 nm/585 nm. (A) Microenvironments in the channel visualized *via* SNARF before and after inverting potential of the biased microelectrodes. Three ROIs were placed in the areas where electrodes were switched (see Fig. 1). (B) Suboptimal pH cycles obtained with 2.5 V amplitude in 50 mM phosphate buffer. As described in the Materials and methods section, pH was monitored ratiometrically with SNARF-4F fluorescence. The colour scheme is given as an alternative interpretation of pH oscillations. (C) Illustrate values of pH assigned at two ROIs *via* SNARF-4F.

immobilized system. This allowed successful switching of triplex DNA conformations (ESI, Fig. S6†).

While the immobilized pMBQ redox system has advantages in keeping the redox components distinct from test solutions, it is less easy to setup and refresh than the equivalent bulk system, especially considering the need to clean electrodes. For most of the subsequent experiments therefore, a bulk solution of benzoquinone/hydroquinone redox components was employed in the pH cycles in a microfluidic channel. The pattern of pH is illustrated over multiple cycles in Fig. 5.

The pH time profiles produced were sensitive to buffer content and the voltage applied (ESI, Fig. S7 and S8†). While the method of SNARF-4F ratio imaging provides information on the pH distribution in flow microreactors under many possible conditions, the electronic induction of pH can potentially induce other processes interfering with the chemistry being studied. In order to separate such effects, we investigated the ability to induce a local pH change in one channel using electrodes, and then have this pH change transfer (*via* diffusion over a hydrodynamic barrier) to a second channel, where it may be used to control complex equilibria and chemical reactions. In the double H-structure (Fig. 1), the flow was significantly slowed down in the top channel (first T-junction upstream substructure "N"). While four positive microelectrodes in the bottom channel were producing an asymmetrically localized low pH microenvironment under steady flow (pH 6.3), the pH of the microenvironment in the top channel decreased non-linearly to *ca.* 5 after 36 min of electrode activation. As a result, pH was switched remotely in the microfluidic reactor *via* diffusive transfer (Fig. 6), without the need for electrode activation in the target channel.

While pH in the "active area" (circled) of the lower channel stabilized at the value 6.3 after 20 min (Fig. 6A, grey plot), the pH in this passive channel reached values low enough to quench SNARF-4F after 40 min of applying voltage in the lower channel. Dual emission of SNARF-4F decreases with decreasing pH and is quenched at pH below 4 (see also Fig. S7†). The sharp drop in fluorescence (black curve) beyond 35 min is likely to be the result of exhausted buffer capacity of the phosphate buffer in the pH range below *ca.* 5.5.

Titrated and electronic pH switching of DNA triplex complexes

A black hole quencher (BHQ) on the third triplex strand allowed us to follow the kinetics of cycles of triplex formation and dissociation in the system H:Q *via* fluorescence quenching (Fig. S1B†). The ss **Y24** was labelled with BHQ-3 at its 3′-end (forming **Q24**, Table 1), which in the antiparallel triplex H:Q would be in the proximity of and quench Alexa647 at the 5′-end of ds **H24**. Fluorescence quenching took 1–2 min in a bulk 1 μM H:Q solution at pH 6.0 (50 mM NaCl) and driving the pH of the solution periodically between 5.0 and 8.0 (by pipetting HCl and NaOH) caused conformational cycles in the H:Q system between unbound and bound (triplex) states as shown in Fig. 7. This was verified by fluorescence quantification of the results of

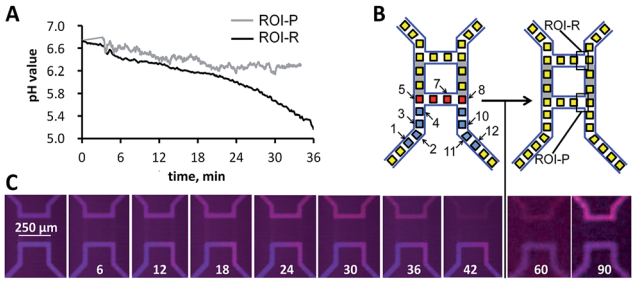

Fig. 6 Remote pH changes using two weakly coupled microfluidic channels. (A) Plots illustrating average local changes of pH in the H-structure at two ROIs under remote control. (B) Electrodes 1–12 were actuated according to the scheme in the lower channel. H^+ ions diffused to the interconnected top microchannel across the hydrodynamic barrier. (C) Ratio imaging and colours representing pH are taken from Fig. 2. The integer labels are times in min and the vertical line indicates the time at which the potential was switched off.

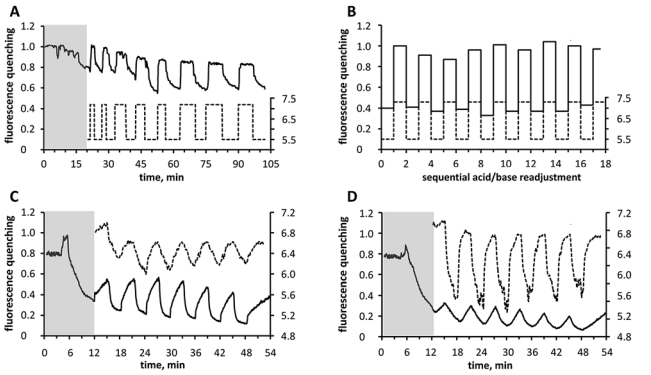

Fig. 7 Reversible triplex switching of DNA H:Q monitored by fluorescence quenching. (A) Changes of pH were performed in 10 µl microwell manually, with addition of 0.1 µl aliquots of 1 M HCl or 1 M NaOH to 0.5 µM DNA ds **H24** and ss **Q24** in 10 mM phosphate buffer. Fluorescence changes were monitored in a fluorescence microscope at 4× magnification, integrated, plotted *vs.* time and smoothed (5 point average). (B) Changes of pH were performed in 1 ml cuvette, with addition of 10 µl aliquots as above, but with 0.5 µM DNA ds **H24**, 1.5 µM ss **Q24** and 50 mM NaCl. (C and D) Electronically controlled pH-mediated molecular switch of triplex in microfluidics at two different locations: (C) lateral to driving electrodes (D) in between driving electrodes. The pH was cycled electronically (1.8 V, *f* 0.0055 Hz) in the system of 0.5 µM DNA ds **H24** and 1.5 µM ss **Q24** in 10 mM phosphate. The microfluidic structures as well as patterns of the electrodes are as in Fig. 1. Measurement locations for pH (broken line) as well as for triplex hybridization (unbroken line) in (C) and (D) were aligned at the same position in the microfluidic channel. Oscillations of pH are plotted *via* broken lines, values of pH in (C) and (D) were assigned using ratio imaging of SNARF-4F (Fig. 2 and S8†).

pH pipetting in a microtiter plate (custom fluorescence setup, Fig. 7A) as well as at a skewed concentration ratio in a 1 ml cuvette (Fig. 7B). The dynamics of fluorescence oscillations over many titration cycles reflects the build up of NaCl concentration (*ca.* 15 mM per cycle) in the system favouring triplex formation (initially only 10 mM sodium phosphate was present in the system). As expected, the accumulation of salt increased the amplitude of fluorescence changes in later cycles (Fig. 7A). The fluorescence of Alexa647 DNA fell when the strands formed triplex DNA H:Q at low pH and recovered at high pH when the strands dissociated (Fig. 7B). As a control, cycling ds **H24** without ss **Q24**, there were no changes of Alexa647 fluorescence observed in the pH range 4–9.

Fluorescence quenching at low pH was incomplete on the switching timescale at the DNA concentration of 0.5 µM. Maximum quenching (80%) was observed for annealed samples at a 3 : 1 ratio of H to Q in a cuvette. The kinetics of triplex cycles was relatively slow ($t_{1/2}$ *ca.* 3 min), but concentration dependent: the hybridization reaction at low pH revealed second order kinetics (Table 2). In the presence of a 3× equivalent of ss **Q24**, the quenching effect was slightly stronger than in the stoichiometric system H:Q. The quenching effect associated with the formation of ts H:Q correlated well with the weight of the triplex peak in CGE (Table 2).

Having established the basic pH cycling of triplex binding in the bulk, we next made use of the quinhydrone redox system (see section above as well as Materials & methods) in order to perform electronically controlled cycles on triplex formation in a microfluidic channel (Fig. 7C and D). To do this we alternated two groups of electrodes in the same channel (see Materials and methods), as in Fig. 5, but here between 0 and 1.8 V in order to maintain the pH levels for more cycles (*cf.* Fig. S8†). Cycling of voltage resulted in stable oscillations of pH in the channel (Fig. 7C and D, dashed curves) and consequent oscillations in triplex formation, monitored by fluorescence quenching (Fig. 7C and D, solid curves). Reversible triplex formation and dissociation was observed *via* cycling pH both between 6.1 and 6.6 (Fig. 7C) as well as between 5.2 and 6.5 (Fig. 7D). The

Table 2 Changes of fluorescence associated with triplex formation at pH 5.0. cuvette assay. Correlation of data on isothermal triplex formation at the same conditions obtained from CGE analysis as well as fluorescence

C_{H24}	C_{Y24} / C_{Q24}	Weight of triplex peak, (%) CGE	Quenching extent, (%)	$t_{1/2}$
0.5 µM	0.5 µM	51 ± 6	55 ± 3	19.0 min
1.0 µM	1.0 µM	52 ± 6	55 ± 3	4.5 min
0.5 µM	1.0 µM	66 ± 7	68 ± 3	10.5 min
2.0 µM	1.0 µM	42 ± 5	✗	✗

switching of pH between 6.1/6.6 (Fig. 7C) was monitored in the ROI-A located 40–60 µm upstream of the working electrodes (see Fig. 1). The amplitude of pH oscillations increased up to 5.2/6.5 (Fig. 7D) in the ROI-B where the potential was switched. Ratiometric analysis of SNARF-4F fluorescence allowed us to separate field dependent concentration effects from pH. Fluorescence traces at ROI-A and B (see Fig. 1 and 5) indicated triplex cycles, with an increasing fraction of triplex as cycles progressed. The threshold pH for triplex formation is 6; so the quenching effect is stronger in the case of cycling pH 5.2/6.5. Although larger oscillations in pH were observed at the central location in D, the influence on triplex formation was less because the fraction of time in the neutral or slightly basic

unbound state was too low. Cycling pH between 6 and 4 at ROI-C and D (Fig. 1) revealed irreversible triplex formation (data not shown).

The observed fluorescence oscillations in triplex cycles fit reversible changes of pH very well: at low pH we observed quenching and at high pH recovery of Alexa647 fluorescence induced by complex formation and dissociation. It was demonstrated that pH could be modulated *via* the electrode configuration, depending on the distance from the actuated microelectrodes.

The extent of quenching in the microfluidic channel was compared with values from the bulk experiments. At the maximum quenching extent, observed in the bulk experiment, the normalized fluorescence intensity of Alexa647 in the triplex f_0 reached a value of 0.2, when the ratio of the pre-annealed strands Q to H was more than 3. Under electronic control in the microfluidic system, f_0 approached a value of 0.2 at ROI-A and 0.1 at ROI-B. Excess of the third strand caused better triplex binding as checked separately by CGE (Fig. 3B).

Triplex molecular ligation triggered electronically in microfluidic channels

The next step towards electronic DNA reaction control is to use the pH switch to control DNA-ligation on a double stranded template *via* triplex formation (Fig. S1C†). As above, the double H-structure (Fig. 1 and 6) was chosen to perform pH changes for these triplex-mediated ligation experiments (Fig. 8). As a ligation chemistry, we chose the recent rapid S–S ligation scheme.[43] Real-time monitoring of the reaction was possible using the quencher leaving group system, designed for that system, involving Alexa488 and Dabcyl (see Materials and methods, Fig. S1D†). The stability of Alexa488 labeled DNA was investigated separately, and it was found that it undergoes a complete quenching transition at pH 5–4.

We first investigated electrostatic impact on the fluorescence changes without ligation. As follows from Fig. 9A, DNA attracted to positive microelectrodes was quenched. Release of the potential caused fluorescence recovery associated with DNA diffusion until the initial concentration of DNA was regained. Electronically induced ligation was studied first in a single channel under proximal electrode control (Fig. 9A, black unbroken curve) before turning to remote switching of ligation in a second channel (Fig. 9B, black curve). The changes of fluorescence *vs.* time reflected the release of the quencher from the oligonucleotide upon ligation, but could be also partially

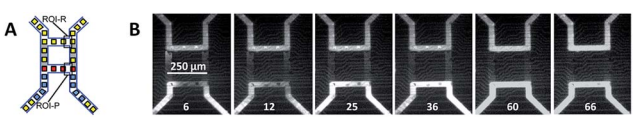

Fig. 8 Switching of template-directed ligation in a microfluidic channel at 1.8 V. (A) The 12-microelectrode array (1–12) was actuated as described in the Fig. 6. Fluorescence profiles were recorded at two ROIs corresponding to the both channels, proximal and remote. (B) Monitoring of fluorescence changes in two diffusively coupled microfluidic channels mediated by the active electrode configuration in lower channel (10-fold magnification).

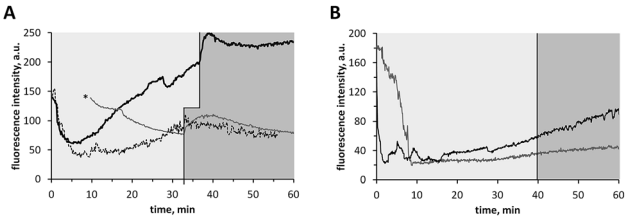

Fig. 9 Kinetics of disulfide DNA ligation reaction in Q/QH_2 redox system under local (A) and remote (B) electrode control, 1.8 V. (A) Template directed DNA ligation, (hairpin **H53** and ss DNA **P12**, **S12**, unbroken black line) traced by fluorescence, compared with controls without ligation partner ss DNA **S12** (broken line), and without template **H53** (grey line). Initial changes are associated with an electrostatic attraction of **P12** to positive microelectrodes. (B) Templated (black) and non-templated (grey) DNA ligation under remote control in the H-structure (see text and Fig. 6). Vertical grey shading indicates period when electrode control was switched off. See Materials and methods as well as Fig. 1 for detailed methods.

affected by DNA concentration changes near the positive microelectrodes. To resolve these effects, we also followed fluorescence relaxation traces recorded following electrode switch off (greyed region in Fig. 9). They had a similar initial profile in Fig. 9A but the constant growth of the fluorescence output with electrode activation occurred only in the presence of template.

The quantification of ligation was complicated by an initial drop in fluorescence due to the induced redox reaction, but a clearly separated subsequent time period of strong fluorescence enhancement, that only occurred in the presence of the hairpin template **H53**, revealed that the system could indeed be used to show electronically induced DNA ligation.

The initial fluorescence drop was reproduced in most experiments at 1.8 V (20–100% duty cycle, see Materials and methods). For longer active duty cycles, the fluorescence drop was seen also in the remote channel (Fig. 9B). Reversible quenching at low pH is associated with observed SNARF-4F fluorescence quenching (Fig. 6C and S7†), and self-quenching. In order to produce a low pH for ligation in the buffered system, electrodes were switched on for 30–40 min. The irreversible component of initial fluorescence loss may result from unspecific binding of DNA to gold surfaces coupled with surface plasmon resonance. The more electrodes were actuated, the greater fluorescence loss was observed. There was no significant fluorescence enhancement observed in the case of the background reaction without template, whereas in the presence of template, the initial fluorescence drop was followed by strong fluorescence enhancement. The fluorescence changes associated with locally controlled DNA ligation in the presence of the template were 3-fold stronger than for the non-templated case (see Fig. 9A). After the electrodes were switched off, fluorescence can continue to increase through DNA migration to the remote location (see Fig. 9B). No significant fluorescence change associated with electrostatic concentration of the DNA (12-mer) was observed in the benzoquinone/hydroquinone system. The time scale 45–60 min (Fig. 9) is in the correct range for the ligation reaction (as usual, somewhat slower than in bulk).

Turning to the investigation of the remote ligation control case, after 1 h monitoring of the reaction in the bottom channel we kept electrodes switched on, and observed fluorescence changes in the top channel (Fig. 8). The experimental arrangement is similar to that employed in the remote channel pH switching section above (see also Materials and methods, including flushing procedure). As in the in-channel ligation switching results above, a quick initial drop in fluorescence was observed both in the absence as well as in the presence of the hairpin DNA template (Fig. 9B). However a subsequent increase in fluorescence was only observed in the presence of template. The remote control of DNA ligation significantly reduced the perturbation from electrodes to fluorescence reporting (*e.g. via* surface quenching).

Discussion

We first discuss the main system choices made at each of four stages of electronic control: electrode locations, pH system, triplex system and ligation system.

Although the electronic control was demonstrated to work with in-channel local electrodes for each of the above three chemical processes, the complications induced by local redox chemistry and electrophoretic transport and concentration make the investigation of remote electrode switching highly desirable. Remote electrode switching has been found useful already for electrophoretic separations in microfluidic systems,[45] usually in connection with placing the electrodes in lateral bays. The special feature of our architecture, employing a shallow ledge opening to create a high hydrodynamic resistance barrier, allows relatively independent hydrodynamic control of flows in the driving and passive channels.[13,51] For example flows can be started and stopped in one channel without removing material in the other. The symmetric nature of our setup also allows the roles of the channels to be reversed, by activating otherwise passive electrodes in the second channel. This architecture enables complex geometries to be designed without significant branching other than over hydrodynamic barriers, simplifying both the filling and flow control processes, and this has allowed us to design more complex microfluidic reactors for electronic chemical cells. Since the hydrodynamic resistance of openings scales cubically with the smallest dimension, it is relatively straightforward to use two level PDMS microfluidics without high resolution to generate well pressure-separated channels (see Materials and method for details).

We had initially anticipated that an immobilization of the pH redox system would open additional capabilities in flow through systems. Indeed, both the immobilized redox system, pMBQ, as well as the bulk redox mixture benzoquinone/hydroquinone that we investigated allowed pH control patterns to be created through redox reactions, below the thresholds for water electrolysis. The latter is deprecated both because of unwanted side reactions as well as because of unwanted bubble creation. Stable pH oscillations were orchestrated *via* microelectrodes and the extent of pH changes was calculated *via* ratio imaging of SNARF-4F. The optimal pH shift, which causes the hybridization switch of the triplex system H:Y, is between pH 6 and 7. Although cycles of electrode potential in the immobilized pMBQ system affected pH of the media to the same or greater extent as compared with the bulk system, the replenishable nature of the bulk quinhydrone pH switching system made investigation of the different conformational and reactive switches in microsystems more tractable. In particular, we made extensive use of the switchable patterns of pH in the electronic control of DNA triplex mediated processes.

Concerning the choice of triplex system for electronically switched hybridization: the separation and online monitoring of DNA complexes in CGE revealed several disadvantages of the system Y:R:Y, such as low stability of the triplex during migration of strands and the close location of the dyes due to additional interactions between the strands (see ESI†). The hairpin DNA template H24, because of its bimolecular rather than termolecular nature, showed enhanced stability as triplex DNA. The H:Y system also had a better-controlled labelling scheme, with less interference between the labels, which in turn made the interpretation of the observed results clearer. Actually, the hairpin DNA plus single strand system is a closer analogue to standard DNA duplex hybridization, but with the advantage that dehybridization can be induced at near neutral pH and low ionic strength (whereas pH over 11.5 is required for ds DNA denaturation) and without destruction of the DNA (*e.g.* depurination at pH 4). The use of dye quenching to monitor triplex formation between the hairpin and single strand is in many respects similar to the standard use of dye–quench pairs for DNA hybridization in double strands. In the triplex complex switching experiment, there is an additional quenching effect that appears to be associated with greater triplex yield in the system due to the higher population of DNA in the vicinity of positive microelectrodes. However, since our signal is a quenching signal, this may also be partially associated with gold surface plasmon quenching.[65,66] Triplex DNA can also be tuned to switch at different pH values depending on the sequence.[67]

The use of relatively short DNA building blocks for ligation (12-mers, see also Materials and methods) was chosen to allow partially reversible binding and facilitate possible turnover in ligation or later replication. In the pH range of 5–6, we expect a minimum of 30% of the 12-mers to hybridize the hairpin template *via* triplex interactions. The interpretation of in-channel ligation experiments is complicated by the fact that the attraction of DNA to the positive microelectrodes may change the concentration ratio between 12-mers and the hairpin template and so affect the equilibrium, *i.e.* shift it towards triplex binding.

Conclusions

This paper established that local microelectrodes in microfluidic channels can be used to electronically control DNA hybridization, dehybridization and ligation in triplex structures *via* controlled non-electrolytic pH switching in a quinhydrone redox couple.[44] Changes in pH were monitored quantitatively using SNARF-4F and ratiometric imaging of fluorescence. Changes in triplex to duplex conformations induced locally *via* pH were monitored by fluorescence quenching using Alexa647

and BHQ. Changes in ligation were monitored by the quencher leaving group strategy and disulphide chemistry developed by Patzke *et al.*[43] Since electrodes induce a variety of local effects including concentration, migration and Faradaic reactions, we also established that the electronic switching of DNA conformations and reactions could be carried out remotely in a diffusively coupled second channel. This may find wider application in biotechnology, in DNA computations and control of self-assembly. The results of this paper can be combined with smart gels in microfluidic systems, that can sequence-selectively transport DNA in a DNA-linked triblock copolymer hydrogel.[49]

The method presented here is designed to support sampling of the reaction products after a DNA replication cycle, fast separation, online monitoring and the analysis of the contents. Quick system response, low diffusion rates as well as long time scale experiments make electronically controlled pH cycles useful for triggering many pH responsive systems beyond triplex based DNA ligation studied here as a step towards electronic chemical cells. In particular, quadruplex and i-motif systems, as employed in ref. 68 should also be switchable in the same pH range, opening the door to a variety of amplification and sensing strategies. We expect that this work will help foster the transition to spatially coupled transport and reaction systems under electronic control to expand the repertoire of DNA processing and synthetic biological systems available.

This work is one component in the development of electronic chemical cells, utilizing DNA as an informational molecule as well as the molecule being synthesized. While enzymatic systems (involving proteins) are powerful in DNA processing, non-enzymatic systems hold the promise of organizational closure, enabling complete self-construction of all informational molecules, without the formidable task of having to synthesize the protein translation system to produce enzymes. The electronic control of the chemical manipulations of DNA is intended to contribute to DNA replication in microfluidic structures allowing selective positioning and separations of the newly synthesized DNA.[13]

Acknowledgements

The authors wish to thank Jana Bagheri-Maurer, Thomas Maeke, Tarik Abdulazim and Abhishek Sharma for their assistance with biochemical tests, microreactor fabrication, implementation and set-up. Volker Patzke synthesized the building blocks for disulphide ligation for use in a joint investigation of rapid triplex-based DNA ligation (to appear elsewhere). The authors also wish to thank Volker Patzke, Matthias Pankau and Guenther von Kiedrowski for helpful discussions. This research has received funding from the European Union's Seventh Framework Programme for research, technological development and demonstration under grant agreements no. 222422 (ECCell) and 249032 (MATCHIT).

Notes and references

1 N. C. Seeman, *Nature*, 2003, **421**, 427–431.
2 N. C. Seeman, *Trends Biochem. Sci.*, 2005, **30**, 119–125.
3 L. M. Adleman, *Science*, 1994, **266**, 1021–1024.
4 J. S. McCaskill, *Biopolymers*, 1990, **29**, 1105–1119.
5 G. Seelig, D. Soloveichik, D. Y. Zhang and E. Winfree, *Science*, 2006, **314**, 1585–1588.
6 K. Montagne, R. Plasson, Y. Sakai, T. Fujii and Y. Rondelez, *Mol. Syst. Biol.*, 2011, **7**, DOI: 10.1038/msb.2011.12.
7 M. P. Robertson and G. F. Joyce, *Cold Spring Harbor Perspect. Biol.*, 2010, **4**, 1–24.
8 G. von Kiedrowski, *Bioorg. Chem. Front.*, 1993, 113–146.
9 M. Kindermann, I. Stahl, M. Reimold, W. Pankau and G. von Kiedrowski, *Systems Chemistry*, 2005, **44**, 6750–6755.
10 D. Zhang, A. Turberfield, B. Yurke and E. Winfree, *Science*, 2007, **318**, 1121–1125.
11 C.-H. Lu, F. Wang and I. Willner, *J. Am. Chem. Soc.*, 2012, **134**, 10651–10658.
12 I. Willner, B. Shlyahovsky, M. Zayats and B. Willner, *Chem. Soc. Rev.*, 2008, **37**, 1153.
13 P. F. Wagler, U. Tangen, T. Maeke and J. S. McCaskill, *BioSystems*, 2012, **109**, 2–17.
14 N. Baran, A. Lapidot and H. Manor, *Proc. Natl. Acad. Sci. U. S. A.*, 1991, **88**, 507–511.
15 A. Dayn, G. M. Samadashwily and S. M. Mirkin, *Proc. Natl. Acad. Sci. U. S. A.*, 1992, **89**, 11406–11410.
16 G. M. Samadashwilyl, A. Dayn and S. M. Mirkin, *EMBO J.*, 1993, **12**, 4975–4983.
17 M. D. Frank-Kamenetskii and S. M. Mirkin, *Annu. Rev. Biochem.*, 1995, **64**, 65–95.
18 J. Bernues, R. Beltran, J. M. Casanovas and F. Azorin, *EMBO J.*, 1989, **8**, 2087–2094.
19 G. E. Plum, D. S. Pilch, S. F. Singleton and K. J. Breslauer, *Annu. Rev. Biophys. Biomol. Struct.*, 1995, **24**, 319–350.
20 G. E. Plum and K. J. Breslauer, *J. Mol. Biol.*, 1995, **248**, 679–695.
21 M. Mills, P. B. Arimondo, L. Lacroix, T. Garestier, C. Hélène, H. Klump and J. L. Mergny, *J. Mol. Biol.*, 1999, **291**, 1035–1054.
22 N. Sugimoto, P. Wu, H. Hara and Y. Kawamoto, *Biochemistry*, 2001, **40**, 9396–9405.
23 C. H. Tung, K. J. Breslauer and S. Stein, *Nucleic Acids Res.*, 1993, **21**, 5489–5494.
24 A. Eick, F. Riechert-Krause and K. Weisz, *Bioconjugate Chem.*, 2010, **21**, 1105–1114.
25 Y. Chen, S.-H. Lee and C. Mao, *Angew. Chem.*, 2004, **43**, 5335–5338.
26 Y. Chen and C. Mao, *J. Am. Chem. Soc.*, 2004, **126**, 8626–8627.
27 B. Kolaric, M. Sliwa, M. Brucale, R. A. L. Vallée, G. Zuccheri, B. Samori, J. Hofkens and F. C. De Schryver, *Photochem. Photobiol. Sci.*, 2007, **6**, 614.
28 V. N. Potaman and V. N. Soyfer, *Triple-Helical Nucleic Acids*, Springer, 1995.
29 J. Tumpane, R. Kumar, E. P. Lundberg, P. Sandin, N. Gale, I. S. Nandhakumar, B. Albinsson, P. Lincoln, L. M. Wilhelmsson, T. Brown and B. Nordén, *Nano Lett.*, 2007, **7**, 3832–3839.
30 K.-I. Haruna, H. Iida, K. Tanabe and S.-I. Nishimoto, *Org. Biomol. Chem.*, 2008, **6**, 1613–1617.

31 Y. H. Jung, K.-B. Lee, Y.-G. Kim and I. S. Choi, *Angew. Chem.*, 2006, **118**, 6106–6109.
32 Y. Dong, Z. Yang and D. Liu, *Acc. Chem. Res.*, 2014, **47**, 1853–1860.
33 T. Li and M. Famulok, *J. Am. Chem. Soc.*, 2013, **135**, 1593–1599.
34 H. A. Day, P. Pavlou and Z. A. E. Waller, *Bioorg. Med. Chem.*, 2014, **22**, 4407–4418.
35 A. T. Winfree, *Science*, 1972, **175**, 634–636.
36 A. N. Zaikin and A. M. Zhabotinsky, *Nature*, 1970, **225**, 535–537.
37 Y. Hara, S. Maeda, T. Mikanohara, H. Nakagawa, S. Nakamaru and S. Hashimoto, in *Smart Actuation and Sensing Systems – Recent Advances and Future Challenges*, InTech, 2012, pp. 311–344.
38 S. Sasaki, S. Koga, R. Yoshida and T. Yamaguchi, *Langmuir*, 2003, **19**, 5595–5600.
39 D. A. Rusling, I. S. Nandhakumar, T. Brown and K. R. Fox, *ACS Nano*, 2012, **6**, 3604–3613.
40 T. Li and K. C. Nicolaou, *Nature*, 1994, **369**, 218–221.
41 Y. Z. Xu and E. T. Kool, *J. Am. Chem. Soc.*, 2000, **122**, 9040–9041.
42 H. Abe, Y. Kondo, H. Jinmei, N. Abe, K. Furukawa, A. Uchiyama, S. Tsuneda, K. Aikawa, I. Matsumoto and Y. Ito, *Bioconjugate Chem.*, 2008, **19**, 327–333.
43 V. Patzke, J. S. McCaskill and G. von Kiedrowski, *Angew. Chem.*, 2014, **126**, 4306–4310.
44 B. van der Schoot and P. Bergveld, *Sens. Actuators*, 1985, **8**, 11–22.
45 D. Kohlheyer, J. C. T. Eijkel, S. Schlautmann, A. Van Den Berg and R. B. M. Schasfoort, *Anal. Chem.*, 2008, **80**, 4111–4118.
46 N. Klauke, P. Monaghan, G. Sinclair, M. Padgett and J. Cooper, *Lab Chip*, 2006, **6**, 788–793.
47 O. Kreft, A. Javier, G. Sukhorukov and W. Parak, *J. Mater. Chem.*, 2007, **17**, 4471–4476.
48 R. L. Rill, Y. J. Liu, D. H. Van Winkle and B. R. Locke, *J. Chromatogr.*, 1998, **817**, 287–295.
49 P. Wagler, G. A. Minero, U. Tangen, J. W. D. Vries, D. Prusty, M. Kwak, A. Herrmann and J. S. McCaskill, *Electrophoresis*, 2014, submitted.
50 P. Wagler, U. Tangen and T. Maeke, *Smart Mater. Struct.*, 2003, **12**, 757–762.
51 U. Tangen, P. Wagler, S. Chemnitz, G. Goranovic, T. Maeke and J. McCaskill, *ComPlexUs*, 2006, **3**, 48–57.
52 S. Chemnitz, U. Tangen, P. Wagler and T. Maeke, *Chem. Eng. J.*, 2008, **135**, 276–279.
53 T. Fujii, *Microelectron. Eng.*, 2002, **61–62**, 907–914.
54 G. M. Whitesides, *Nature*, 2006, **442**, 368–373.
55 S. Sia and G. Whitesides, *Electrophoresis*, 2003, **24**, 3563–3576.
56 P. F. Wagler, U. Tangen, J. Ott and J. S. McCaskill, *IEEE Trans. Compon., Packag., Manuf. Technol.*, 2014, **5**, 291–300, DOI: 10.1109/tcpmt.2015.2395815.
57 U. Tangen and T. Maeke, ngbiopro software, RUB-BioMIP, 2012, http://fp7matchit.eu/uploads/images/software_repository/MATCHIT-CTRL-ng_biopro_20130403.tar.gz.
58 B. R. Eggins, *J. Chem. Soc. D*, 1969, 1267–1268.
59 I. Rubinstein, *J. Am. Chem. Soc.*, 1981, **103**, 512–516.
60 J. K. Leland and M. J. Powell, *J. Electrochem. Soc.*, 1990, **137**, 3127.
61 A. Arora, J. C. T. Eijkel, W. E. Morf and A. Manz, *Anal. Chem.*, 2001, **73**, 3282–3288.
62 S. F. Singleton and P. B. Dervan, *Biochemistry*, 1993, **32**, 13171–13179.
63 K. H. Nam, S. Abhiraman and R. M. Wartell, *Nucleic Acids Res.*, 1999, **27**, 859–865.
64 N. Panchuk-Voloshina, J. Bishop-Stewart, M. K. Bhalgat, P. J. Millard, F. Mao, W. Y. Leung and R. P. Haugland, *J. Histochem. Cytochem.*, 1999, **47**, 1179–1188.
65 K. B. Cederquist and C. D. Keating, *Langmuir*, 2010, **26**, 18273–18280.
66 J. N. Murphy, A. K. H. Cheng, H.-Z. Yu and D. Bizzotto, *J. Am. Chem. Soc.*, 2009, **131**, 4042–4050.
67 A. Idili, A. Vallée-Bélisle and F. Ricci, *J. Am. Chem. Soc.*, 2014, **136**, 5836–5839.
68 M. Frasconi, R. Tel-Vered and J. Elbaz, *J. Am. Chem. Soc.*, 2010, **132**, 2029–2036.